# MECHANICAL AND CORROSION STUDIES OF FRICTION STIR WELDED AA8090 ALLOY

**A SYNOPSIS**

*Submitted by*


**C. SHYAMLAL**

**(Reg. No. 2019141113)**


*in partial fulfillment for the award of the degree*

*of*

DOCTOR OF PHILOSOPHY


**DEPARTMENT OF MECHANICAL ENGINEERING**

**SCHOOL OF MECHANICAL, AERO, AUTO AND CIVIL ENGINEERING**

**KALASALINGAM ACADEMY OF RESEARCH AND EDUCATION**

(DEEMED TO BE UNIVERSITY)

**ANAND NAGAR, KRISHNANKOIL – 626 126**

**TAMIL NADU, INDIA**


**NOVEMBER 2023**

## 1. INTRODUCTION

Aluminium is lighter than steel. The density of aluminium is one-third the density of steel. Further, aluminium exhibits high corrosion resistance due to the formation of passivating film of aluminium oxide upon exposure to atmosphere. The aluminium is slowly replacing steel in many sectors particularly in aerospace constructions in the case of cryogenic fuel tanks where aluminium lithium alloy is employed. The alloying additions such as Li, Cu, Mg, Ti in the aluminium has made the alloy heat treatable and light weight. Further these alloying additions have made aluminium much stronger and formable. The advent of electric vehicles has increased the usage of aluminium since light weight construction is the specific necessity. Aluminium alloys are broadly classified into heat treatable and non-heat treatable alloys. The properties improve with reference to the grain size, the precipitate morphology [1] and the density of dislocations. In automobile, the most commonly used aluminium alloys are AA2xxx, AA5xxx, AA6xxx and AA7xxx because of its environment friendliness and better alternative to steel. FSW offers better mechanical properties for light materials like aluminium, magnesium alloys and aluminium based composites [2], [3]. Particularly in the aerospace industry and in the manufacturing of electric vehicles, the requirement is light weighting and better weld quality. The light-weight aluminium lithium alloys have been employed in the airplane and aerospace structure construction to reduce the density of the structure and also to elevate the elastic modulus [4] and strength of the joint which will make the structure light. The aerospace firms have focused on the alloys which will provide good service life, lesser corrosion resistance, good damage tolerance [5] and good mechanical properties in the outer structure of the aircraft/rocket fuel tank. AA8090 T87 second generation aluminium lithium alloy (the alloy taken for investigation) which contains 2.3 wt.% Li, aids in reducing the weight of the structure by reducing the density of the material. Cu, Mg and Li are the main alloying elements in this alloy whose addition helps in forming hardening precipitate Al-Cu-Li, Al-Cu-Mg, Al-Li-Mg, Al-Li [6]. Table 1 displays different aerospace alloys. Among the alloys listed in the table, AA8090 alloy has lesser Cu/Li ratio. Hence, Li containing precipitate forms in larger amount in AA8090 than other aluminium alloys.

**Table 1** Chemical composition of aerospace alloys

| Alloy | Cu | Mg | Zn | Li | Cu/Li | Ref. |
|---|---|---|---|---|---|---|
| AA8090 | 1.25 | 0.49 | 0 | 2.27 | 0.55 | [7] |
| AA2050 | 3.6 | 0.38 | 0.12 | 0.98 | 3.67 | [8] |

## 2. LITERATURE REVIEW

This literature review gives the background information related to the friction stir welding of AA8090 alloy and other aluminium lithium alloys. Sivaraj et al. [9] discussed about the tensile strength and hardness distribution in the weld regime. It has been discussed that the artificial aging has improved the hardness and tensile strength. The solution treatment along with artificial aging procedure increased the tensile strength and hardness from 394 MPa to 445 MPa and 125 VHN to 171 VHN. Hence, post weld heat treatment and processing parameters have been used to elevate the efficacy of the joint. Sidhar and Mishra [10] discussed about the aging kinetics for attaining better strength and hardness in the weld joint. The PWHT of more than 30 hrs. aging provided improvement in the micro hardness of the structure and also tensile strength. The artificial aging period of 30 hrs and 160° C has changed the hardness profile from W shaped to flat profile which is the indication of improvement of hardness. Sanjeev kumar et al. [11] discussed about the influence of traverse speed on the effectiveness of the joint. The increment in the traverse from 1 mm/s to 4 mm/s has increased the hardness and tensile strength from 115 VHN to 130 VHN and 300 MPa to 390 MPa. The traverse speed influenced the efficacy of the joint by decreasing the grain size. Meng et al. [12] analysed AA2060 T8 alloy and has been subjected to electrodynamic polarization analysis and found that the stir zone has more corrosion resistance than TMAZ and base metal. The lowest corrosion potential in the stir zone was -991 mV. The Li based precipitates was the reason for this lesser stir zone potential. Li et al. [13] discussed about the variation of strength and defects on varying the welding speeds. The defect formation in the retreating side of the joint occurred during welding of AA2195-T8 aluminium lithium alloy while welding at higher welding speeds as high as 120 mm/min. Zhang et al. [14] detailed about the influence of precipitation and grain morphology during recrystallization. The heat generation between the shoulder and work top surface plays important role in recrystallization and grain generation when the ratio of rotation speed and welding speed is increased.

## 3. RESEARCH GAP

Many researchers have analysed mechanical perspective of aluminium lithium alloys in the areas of tensile strength, microhardness. But investigation on AA8090 T87 aluminium alloy is very scarce. Moreover, flexural and corrosion analysis was not done by researchers on this alloy which is very essential analysis for the use of this alloy in vehicle structures. Also, a novel attempt has been made to improve the efficiency of the weld joint by designing the novel friction stir welding tool. The present work deals with the fabrication of weld joint and its characterization, mechanical analysis and corrosion analysis.

## 4. RESEARCH OBJECTIVE

There are a number of primary goals for which this investigation is carried out:

- Characterization and modification of microstructure by modifying shoulder profile and pin profile.
- To develop the heat treatment procedure for the fabricated joint.
- To analyse the mechanical performance of the joint before and after heat treatment.
- To analyse the precipitates formed before and after corrosion.

## 5. METHODOLOGY

### 5.1 Research methodology

Figure 1 describes the complete workflow of research methodology of the present investigation of friction stir welded AA8090 aluminium alloy.

### 5.2 Nomenclature of weld parameter combination

The notation of weld parameter combination is given below and the table of weld parameters used in this work is shown in Table 2.

SxSy = S1S23

x – 1 to 9 weld parameter combination, y – Shoulder diameter (23 mm)

SxSyNzH = S3S17N1H

x - 3 and 9 weld parameter combination, y – Shoulder diameter (17 mm, 20 mm), z – Tool number, H – Heat treated

**Table 2** Weld parameter combination table

| | **Traverse speed, mm/min.** | | |
|---|---|---|---|
| **Spindle speed, rpm** | **30** | **50** | **70** |
| **700** | 1 | 2 | 3 |
| **900** | 4 | 5 | 6 |
| **1100** | 7 | 8 | 9 |

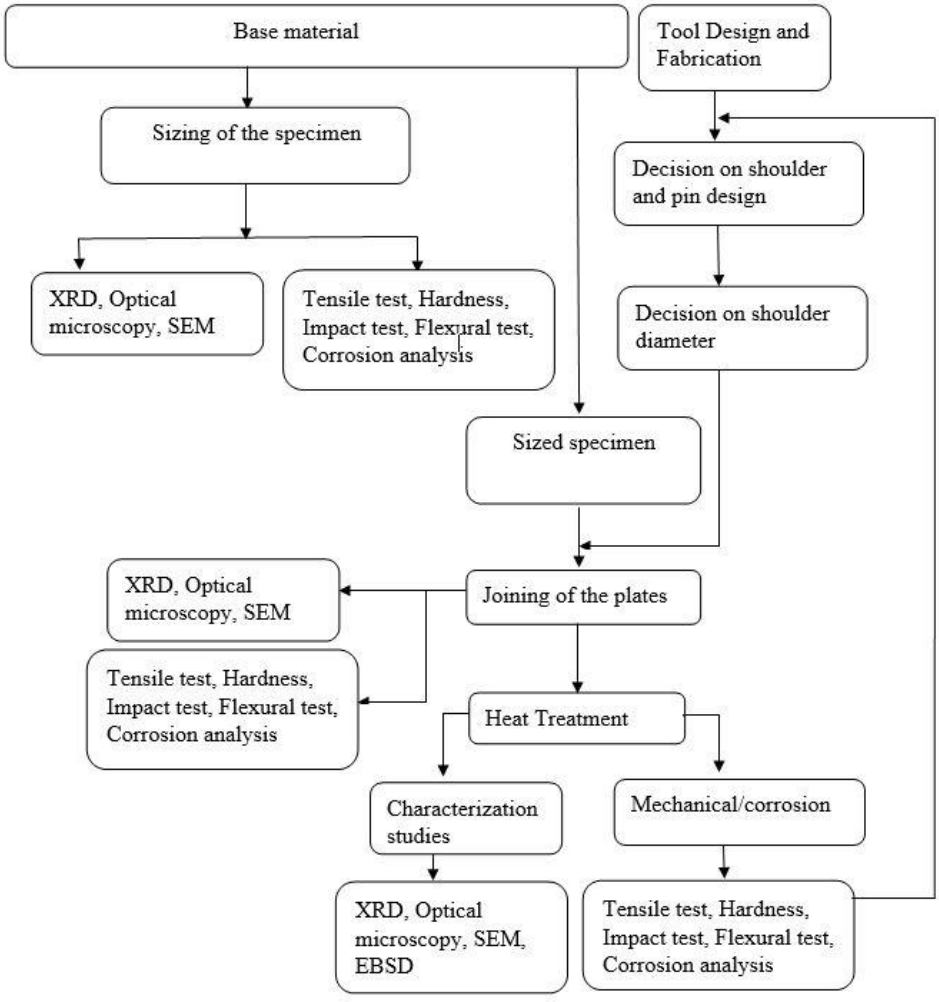
Base material
Tool Design and Fabrication
Sizing of the specimen
Decision on shoulder and pin design
XRD, Optical microscopy, SEM
Tensile test, Hardness, Impact test, Flexural test, Corrosion analysis
Decision on shoulder diameter
Sized specimen
XRD, Optical microscopy, SEM
Joining of the plates
Tensile test, Hardness, Impact test, Flexural test, Corrosion analysis
Heat Treatment
Characterization studies
Mechanical/corrosion
XRD, Optical microscopy, SEM, EBSD
Tensile test, Hardness, Impact test, Flexural test, Corrosion analysis

**Figure 1** Research methodology for friction stir welded AA8090 alloy

# 6. RESULTS AND DISCUSSION

## 6.1 Tool design

Figure 2 (a-b) displays the flat shoulder design tool and scrolled shoulder design FSW tool. The tool has been designed to increase the pulsating action in the joint to improve the efficacy of the joint. Two flats have been fabricated in the pin of the tool to the depth of 1 mm from the circumference of the pin.

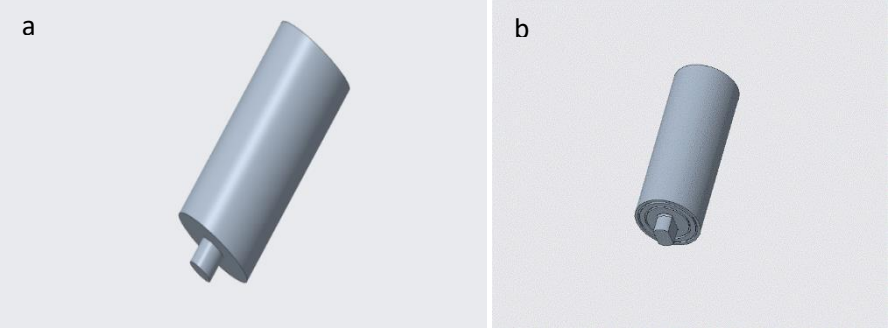


**Figure 2** Friction stir welding tool a. 23 mm tool b. 17 mm, 20 mm tool
H13 tool steel material was used to fabricate the tool.

The tool was hardened to 52 HRC. The scroll with diameter 1 mm was machined to a depth of 0.5 mm in the face of the shoulder to increase the surface area of the tool which increased the heat generation in the interface between the tool surface and the work face.

## 6.2 Results of 23 mm shoulder joint

### 6.2.1 Characterization, mechanical properties and corrosion analysis of 23 mm shoulder diameter weld joint

The micrographs shown in Figure 3 displays SZ, TMAZ and HAZ after welding. It is seen from the above micrographs that Figure 3 (a-c) appeared defect free and the increase in the rotational speed led to defect accumulation/formation in the weld joint from Figure 3 (d-e). The higher rotational speed increased the formation of flash [15] in the joint which also affects the joint effectiveness. The increase in the heat generation in the weld joint is the primary reason for material softening which stood as the reason for the loss of cold work [16] and coarsening of precipitates which were inherent in the base material.

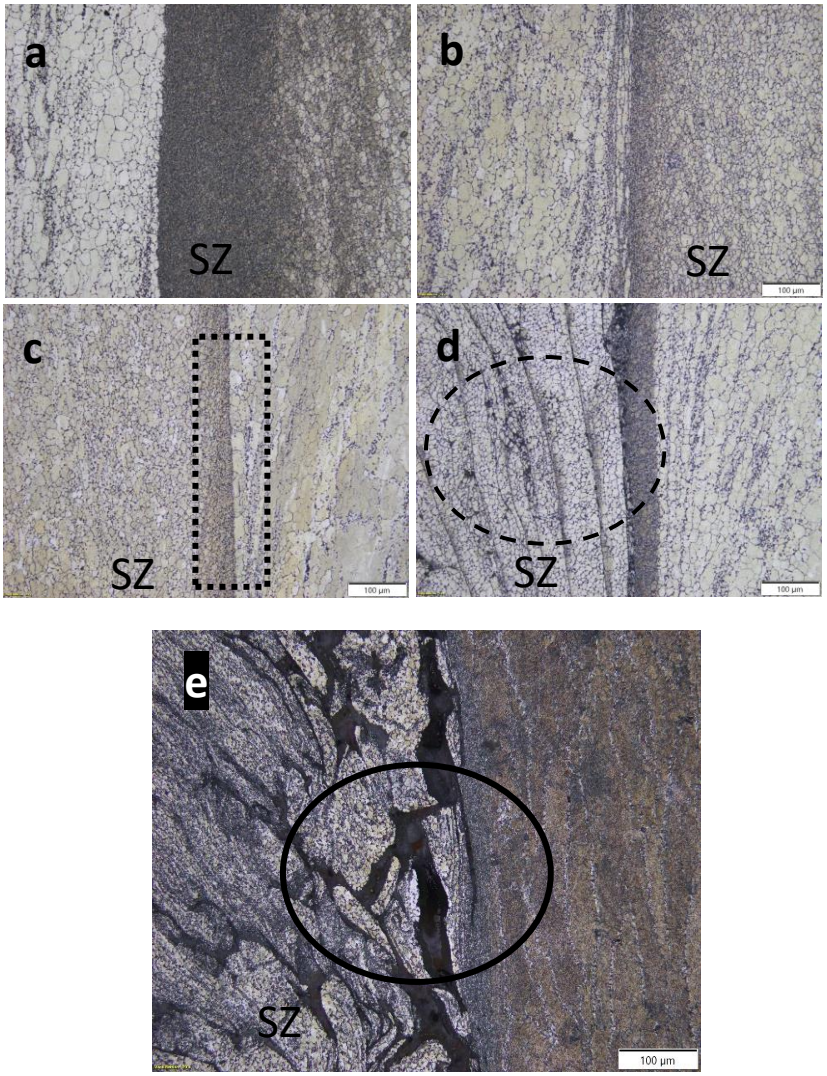


**Figure 3** Microstructure in the interface of SZ and TMAZ (a) S1S23 (b) S2S23 (c) S3S23 (d) S4S23 (e) S8S23

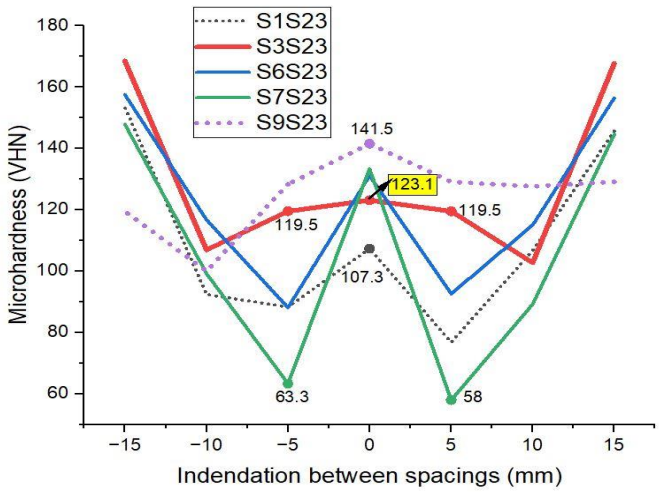


**Figure 4** Microhardness distribution of 23 mm shoulder joint

Low hardness region was observed for 1100 rpm, 30 mm/min. joint, 58 VHN in advancing side and 63.3 VHN in the retreating side. Further, it was observed at a distance of 10 mm from the SZ. Hardness has been increased to 119.5 VHN on either side of the stir zone in S3S23 joint. The stir zone hardness of S3S23 was 123.1 VHN. Highest hardness was obtained for S9S23 joint but displayed asymmetric hardness profile on either side of the SZ as shown in Figure 4. Further from figure, it was found that least hardness was obtained for S8S23 joint (1100 rpm, 50 mm/min.). This was due to the defects accumulation in the joint which was seen from the macrostructure section. Highest hardness was obtained for 1100 rpm, 70 mm/min. joint.

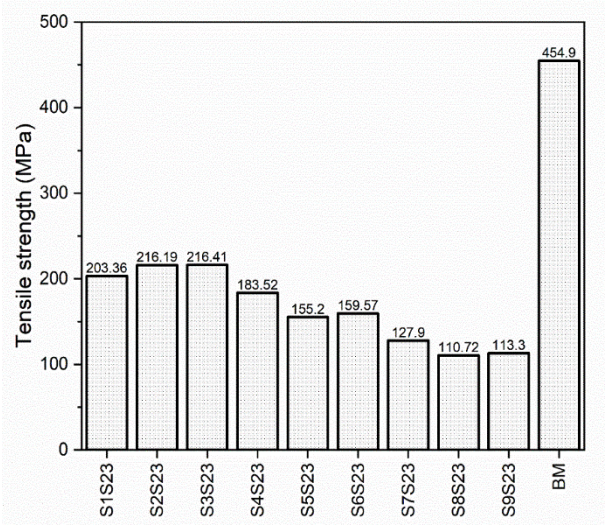


**Figure 5** Tensile strength of 23 mm shoulder joints

Figure 5 shows tensile strength graph of 23 mm shoulder diameter joint. 700 rpm, 70 mm/min. shows highest tensile strength of 216.41 MPa. The least tensile strength of 1100 rpm, 50 mm/min., and 70 mm/min. joint showed more defect accumulation as previously discussed in macrostructure section. The fracture morphology of 700 rpm, 70 mm/min. revealed dimpled fracture morphology as shown in Figure 6.

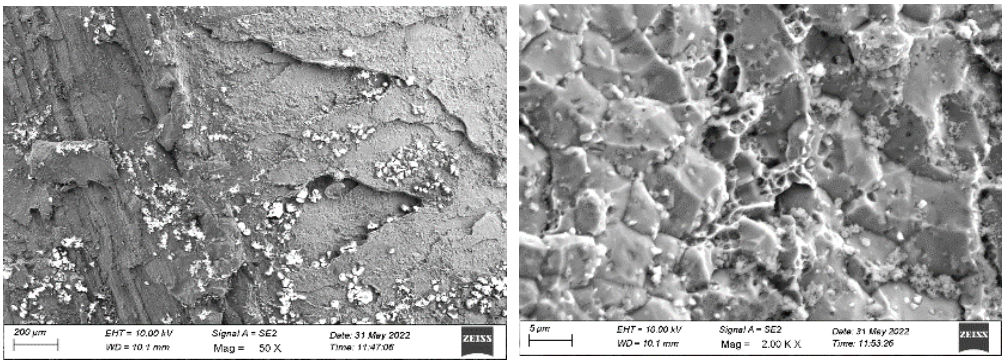


**Figure 6** Fractography of 23 mm shoulder diameter joint.

Tafel curve of 23 mm shoulder joints is shown in Figure 7. Base metal displays highest corrosion resistance of -656.87 mV. 700 rpm, 700 mm/min. joint shows least corrosion resistance of -680.01 mV. 1100 rpm, 70 mm/min. joint shows the corrosion resistance of -662.43 mV. These values dictated variation in the grain size and grain boundary affected the corrosion resistance. As observed from the tafel curve, 1100 rpm joint displayed better corrosion resistance than 700 rpm and 900 rpm joints.

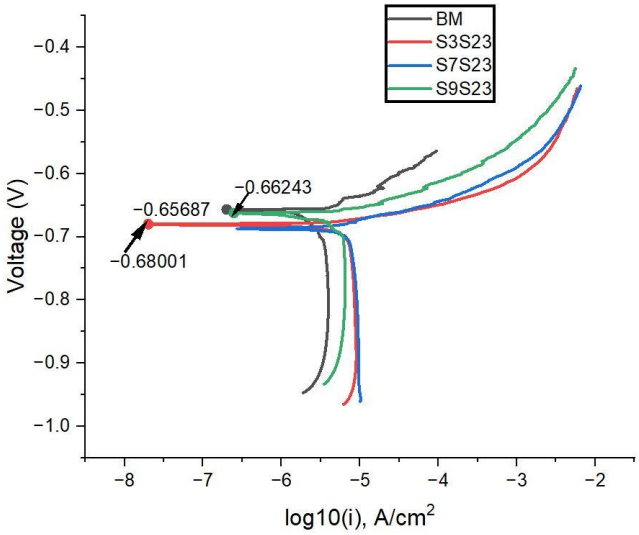


**Figure 7** Tafel curve of 23 mm shoulder joints

### 6.3 Results of 17 mm and 20 mm shoulder joint

#### 6.3.1 Characterization, mechanical properties and corrosion analysis of 17 mm and 20 mm shoulder diameter weld joint

Figure 8 displays the macrostructure of the weld joint. Tunnel type defect appeared in the 1100 rpm, 70 mm/min., 17 mm shoulder diameter and 20 mm shoulder diameter joint. Improper material mixing is the reason for such defects [17]. The defects produced were encircled in black colour.

The increment in the rotational speed from 700 rpm to 1100 rpm induced high amount of friction between tool shoulder and work which led to the generation of large amount of heat and turbulent flow of the plasticized material in the stir zone, thus led to the material softening in SZ, TMAZ and HAZ compared to the base metal. This material softening behavior has led to the increased misalignment of atoms [18] which was reflected as tunnel defect. Further, tunnel defect produced behaved as stress concentration

spot and induced fracture in the specimen as stated by Xu et al. [19] which was reflected in mechanical properties of the joint.

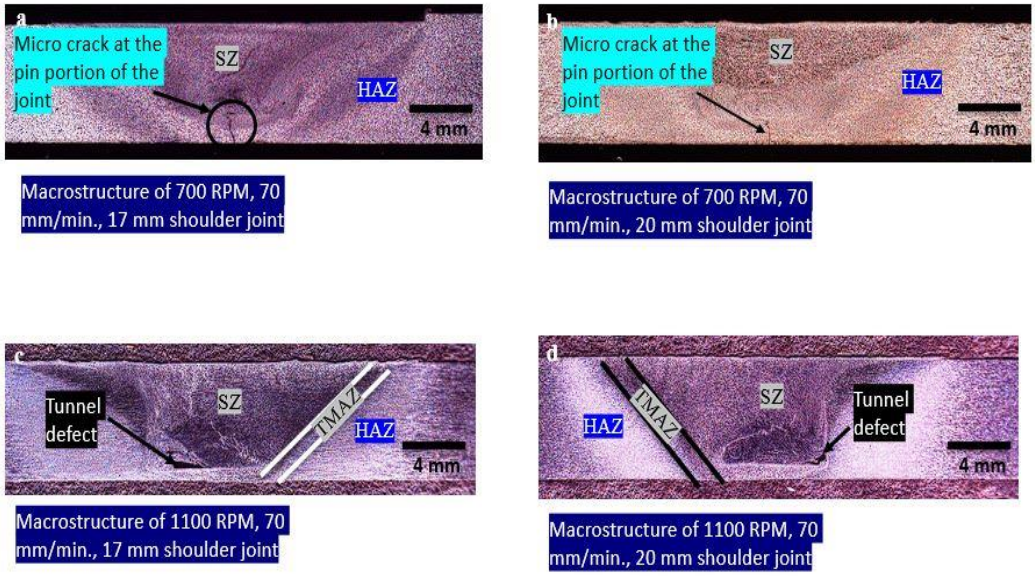


**Figure 8** Macrostructure of the weld. A) S3S17N1 b) S3S20N2 c) S9S17N1 d) S9S20N2

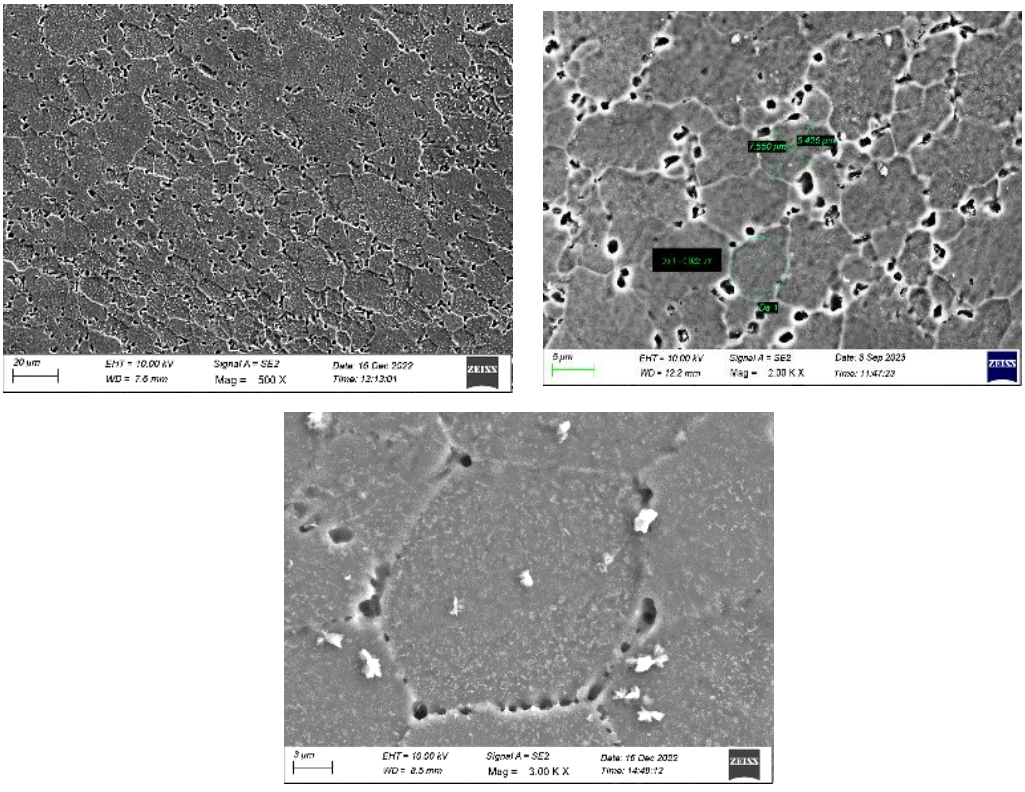

**Figure 9** Microstructure of the weld for 700 rpm, 70 mm/min, 17 mm shoulder diameter

Figure 9 displays the SEM image of the sub surface of the 700 rpm, 70 mm/min. joint using the novel tool. More equi-axed grains were visible in the stir zone in the grain boundaries. The investigation of the precipitates revealed Al and Cu in the precipitate composition and is shown in Figure 9. In the microhardness distribution diagram shown in Figure 10. The hardness of S3S17N1 joint is 105 VHN which has been increased to 145 VHN after heat treatment. This 40 VHN increase was attributed to the aging process carried out at 190 C for 30 hours. Further, the heat treated joints exhibited flat hardness profile relative to non-heat treated joint.

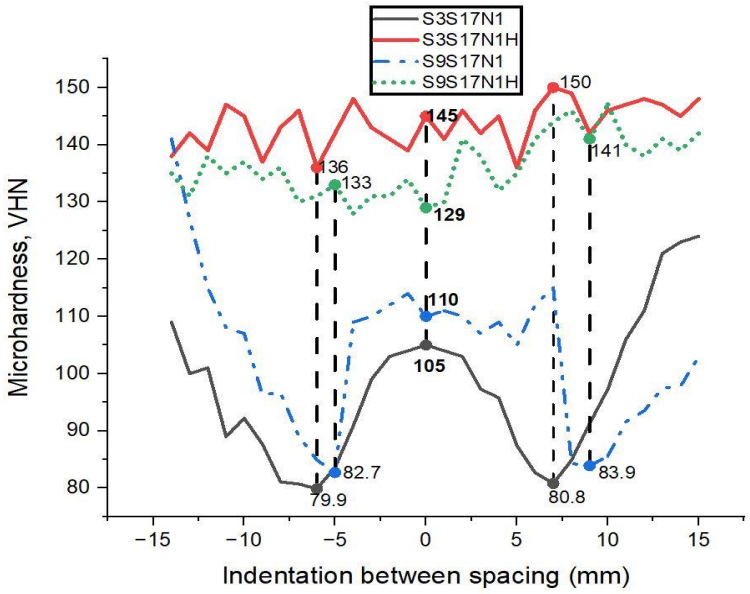


**Figure 10** Microhardness distribution of the weld joint

Tensile strength comparison of weld joint is shown in Figure 11. Tensile strength of the base material is 446.23 MPa with elongation % of 8.67. Tensile strength of 260 MPa was obtained for S3S17N1H Joint. Lowest tensile strength of 203.36 MPa was obtained for S1S23 Joint. Tensile strength of 240 MPa was obtained for S3S20N2H Joint. Tensile strength of 196.88 MPa and 170.79 MPa was obtained for S9S17N1 and S9S20N2 which is 74% more than S9S23 Joint. Hence, the modified tool design aided to improve the joint strength. Lowest tensile strength of 111.12 MPa and 79 MPa was obtained for S9S17N1H and S9S20N2H. This was due to the expansion of defects during heat treatment.

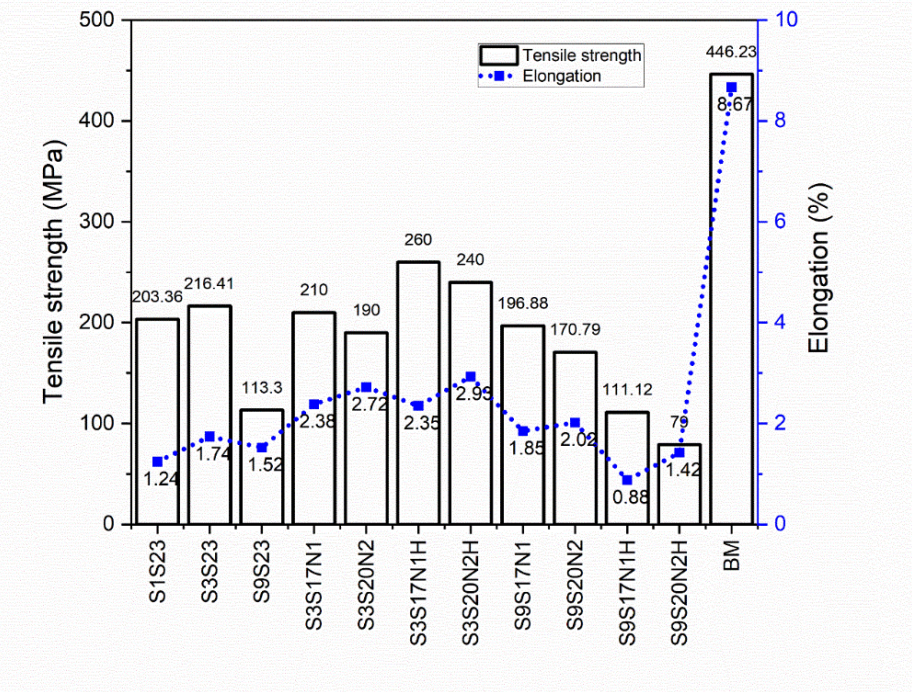


**Figure 11** Tensile strength comparison of the weld joint

Flexural strength of 17 mm shoulder dia. Joint before heat treatment and after heat treatment shows appreciable flexural strength (nearly 90.87% efficacy) as shown in Figure 12. S3S17N1 joint has flexural strength of 622.62 MPa. S3S17N1H joint has flexural strength of 669.59 MPa. S3S20N1, S9S20N2 and S9S20N2H has lowest flexural strength. The appreciable bending efficacy exhibited by S3S17 joints indicate the suitability of the joint to bending applications particularly for aerospace structures and automobile bodies.

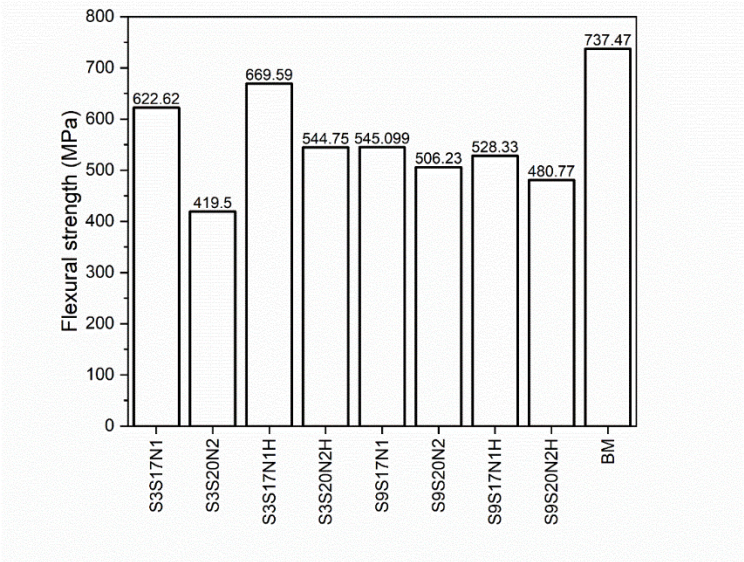


**Figure 12** Flexural strength comparison of weld joint

Figure 13 shows the impact strength comparison of the weld joint welded by 23 mm shoulder diameter and novel tool. The novel tool joint S9S20N2 produced highest impact energy of 8 J. S1S23 joint produced 7.1 J. Hence, highest impact energy was produced by joints produced using novel tool.

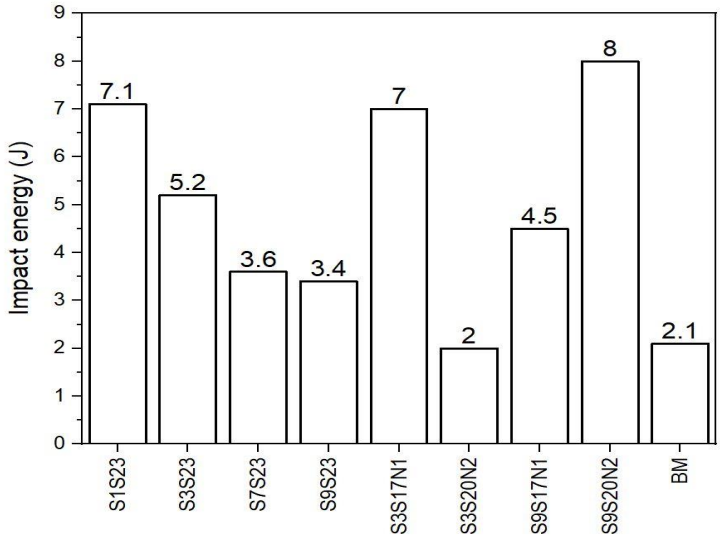


**Figure 13** Impact strength comparison of the weld joint

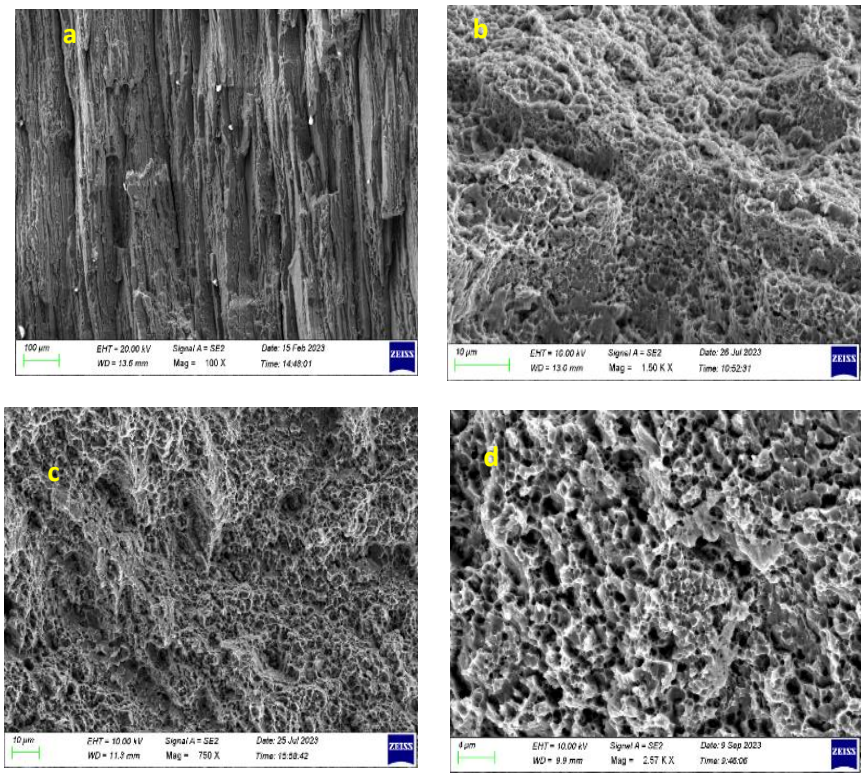


**Figure 14** Fractography a. Base metal b. Tensile failure surface of S3S17N1 joint c. Bending failure surface of S3S17N1 joint d. Impact failure surface of S3S17N1 joint

The fractography analysis shown in Figure 14 revealed that dimples produced by base metal was fibrous in nature. The size of the dimples was more in flexural failure surface than in tensile and impact failure surfaces. This revealed that the flexural performance of the joint is commendable.

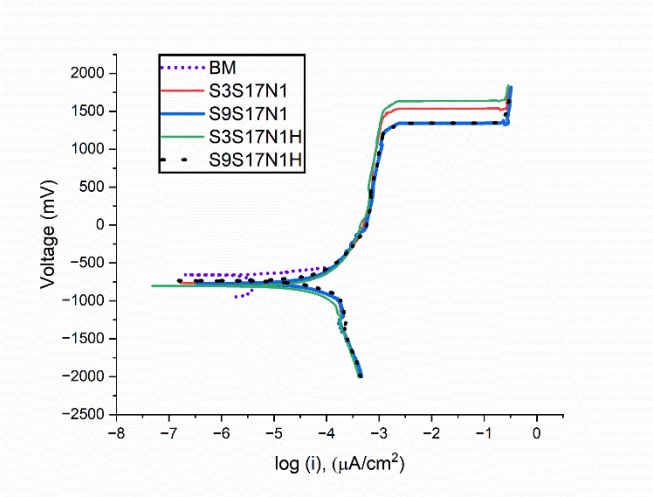


**Figure 15** Tafel curve of 17 mm shoulder diameter joint

The tafel curve shown in Figure 15 shows that the pitting resistance is higher for heat treated and non-heat treated 700 rpm joint. Corrosion rate is very lesser for 700 rpm, 70 mm/min., 17 mm shoulder diameter joint (treated and untreated) than other joints and corrosion pits which are formed due to accelerated corrosion analysis using potentiostat is shown in Figure 16.

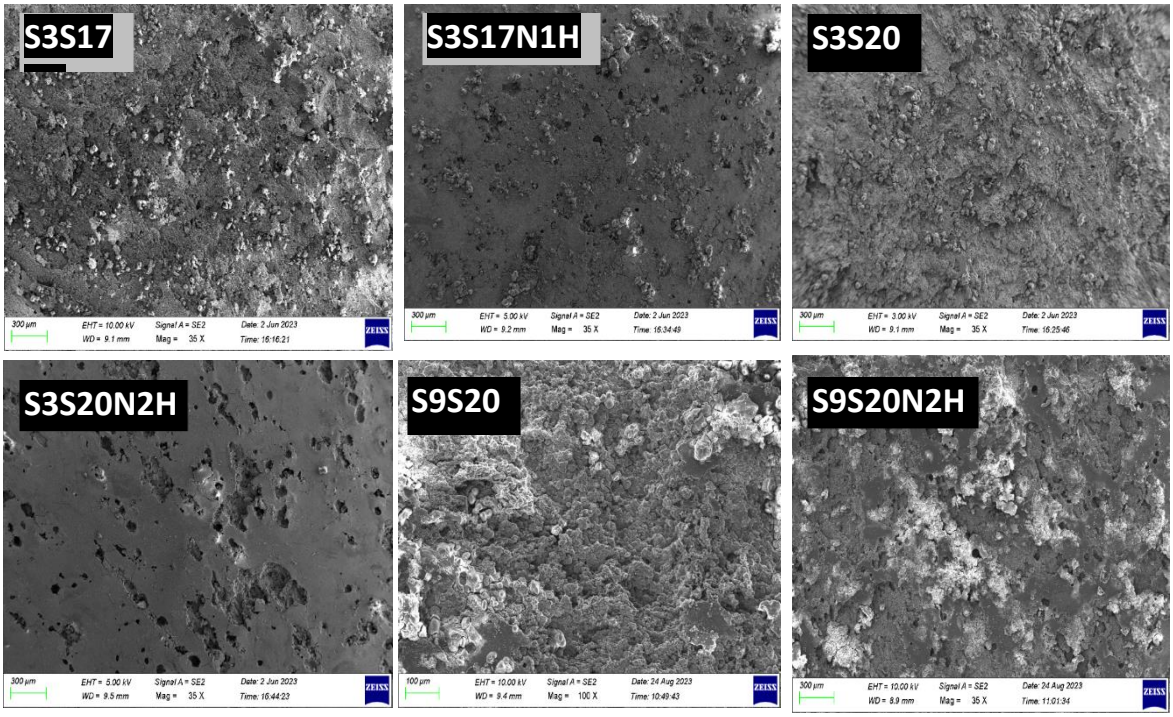


**Figure 16** Sub surface morphology after corrosion

## 7. ORGANIZATION OF THESIS

This thesis is organized and detailed as below:

**Chapter 1** provides an overview of materials used in this work and their classification, especially of aluminium alloys. Furthermore, it discusses about the precipitation behaviour and influencing parameters of friction stir welding process and supporting mathematical expressions.

**Chapter 2** presents a detailed review of the relevant literature on the mechanical properties, corrosion behaviour and the influence of tool design on joint formstion. Based on the literature review, the research gap was identified. The objectives and methodology of this research work are also presented.

**Chapter 3** provides the details of materials used, machines employed for this work, testing conditions employed and the specimens prepared for mechanical and corrosion analysis.

**Chapter 4** provides the details of tool used in this research work, their profiles and selection of design of the tool, advantages of the profiles being chosen for work and outcomes.

**Chapter 5** deals with the mechanical behaviour of the welded joint using tensile, impact, flexural and hardness testing and the morphological characteristics of the fractured specimen using SEM and EBSD. This chapter also deals with corrosion analysis of 23 mm shoulder joint.

**Chapter 6** deals with the mechanical behaviour of the welded joint using tensile, impact, flexural and hardness testing and the morphological characteristics of the fractured specimen using SEM and EBSD. This chapter also deals with corrosion analysis of 17 mm and 20 mm shoulder joint.

**Chapter 7** summarizes the research outcomes from the results and discussions of the experimental work:

**The following evidences has been elicited for 23 mm shoulder joint:**

- The weld joint was subjected to macrostructural studies. Defects such as pin holes, line defects and material discontinuity appeared in the weld joint for 900 RPM, 1100 RPM rotational speeds. 700 RPM joints appeared free of defects.
- In 700 RPM, 30 mm/min. and 70 mm/min. joint elements such as Cu and O dominates and thus formed the precipitate $Al_2Cu$ and $Al_2O_3$.
- Further in S3S23 joint, wt. % Cu appeared to be 51.9 %, wt. % Al was 19.1% in a precipitate inside the grain.
- EBSD studies have been undertaken and found that there is variation in grain size during escalation of rotational speed from 700 RPM to 1100 RPM. Consequently, their grain sizes increased.
- From XRD, it was found that Al, $Al_2CuLi$, $Al_3Li$ and $Al_2Cu$ phases were presented in large amount through out the joint.
- Vickers micro hardness was performed and found that 1100 rpm, 70 mm/min. joint exhibited maximum hardness of 141.5 VHN. The hardness of the stir zone of 700 rpm, 70 mm/min., joint was 123.7 VHN.
- The tensile strength of the base metal was 454.9 MPa. Tensile strength of the stir zone of S3S23 joint was 216.41 MPa which was reduced to 113.3 MPa for S9S23. The reason for this is the generation of defects.
- $E_{corr}$ for S3S23 joint is -680.01 mV. Elements presented were Cl % - 1.86, O %– 35.76, Cu % - 0.9. Chlorine presented in the elemental composition induce damage to sub surface.

**The following evidences has been elicited for 17 mm and 20 mm shoulder joint:**

- Micro cracks were observed in S3S17N1 and S3S20N2 joints. Tunnel defects were observed in S9S17N1 and S9S20N2 joints which was created due to improper bonding of atoms. Abnormal heat generation was the reason for these defects.
- Equi-axed grains were observed in S3S17N1 joints. Non-equi axed grains appeared in S3S17N1T joints and in S3S20N2T which is the effect of heat treatment.
- EDAX mapping of elements revealed the presence of Cu (4.2 %) which dominated Mg and O in S3S17N1 joint which confirmed Al2Cu precipitation.

- Crystallinity index of S3S17N1 was lesser than S3S20N2 joint but greater than heat treated joints.
- The microhardness of S3S17N1 was 105 VHN and that of S3S17N1H was 145 VHN. This 45 VHN increase was attributed to heat treatment which was evident from the flat profile in the hardness distribution.
- The microhardness of S3S20N2/N2H appeared lower than S3S17N1/N1H.
- S3S17N1H exhibited maximum tensile strength of 260 MPa followed by S3S20N2H. Tensile strength of S3S23 was 216.41 MPa followed by S3S17N1.
- Dimpled fracture morphology were obtained for non heat treated joint. Faceted structure were presented in heat treated joints.
- Flexural strength of 669.59 MPa was obtained for S3S17N1H followed by 622.62 MPa for S3S17N1.
- Highest impact strength of 8 J/mm$^2$ was observed for S9S20N2 followed by 7.1 J/mm$^2$ for S1S23, 7 J/mm$^2$ for S3S17N1.
- Dimpled fracture was observed for all specimens fractured due to impact.
- In 700 RPM, 70 mm/min. joint, increase in the shoulder diameter from 17 mm to 20 mm increased corrosion rate from 0.472 mm/year to 5.1 mm/year. Lowest corrosion rate of 0.472 mm/year was observed in S3S17N1H joint.
- In 1100 RPM, 70 mm/min. joint, increase in the shoulder diameter from 17 mm to 20 mm decreased corrosion rate from 4.44 mm/year to 2.002 mm/year. Lowest corrosion rate of 2.002 mm/year was observed in S9S20N2 joint.
- Crystallinity index of corroded joint S9S20N2C was 31.96 % which was lesser than uncorroded S9S20N2 joint (32.96 %).

## REFERENCES

[1] S. Gopalakrishnan and N. Murugan, "Prediction of tensile strength of friction stir welded aluminium matrix TiCp particulate reinforced composite," *Materials & Design,* **32** (1) (2011), 462–467.

[2] O. Gopkalo, X. Liu, F. Long, M. Booth, A. P. Gerlich, and B. J. Diak, "Non-isothermal thermal cycle process model for predicting post-weld hardness in friction stir welding of dissimilar age-hardenable aluminum alloys," *Materials Science and Engineering: A,* **754** (2019), 205–215.

[3] X. Tao, Y. Chang, Y. Guo, W. Li, and M. Li, "Microstructure and mechanical properties of friction stir welded oxide dispersion strengthened AA6063 aluminum matrix composites enhanced by post-weld heat treatment," *Materials Science and Engineering: A,* **725** (2018), 19–27.

[4] M. Agilan, R. Anbukkarasi, T. Venkateswran, PG. Panicker, SV. Kailas, D. Sivakumar, B. Pant, "Studies on friction stir welding of Al-Cu-Li (Aa2195) alloy," *Materials Science Forum,* **830–831** (2015), 274–277.

[5] S. M. O. Tavares, J. F. dos Santos, and P. M. S. T. de Castro, "Friction stir welded joints of Al-Li Alloys for aeronautical applications: Butt-joints and tailor welded blanks," *Theoretical and Applied Fracture Mechanics,* **65** (2013), 8–13.

[6] M. P. Alam and A. N. Sinha, "Fabrication of third generation Al–Li alloy by friction stir welding: a review," *Sadhana,* **44** (2019), 6.

[7] M. H. Abass, F. Mahmud, M. S. Alali, and A. N. Abood, "The effect of annealing and anisotropic behaviour on tensile and fatigue properties of AA 8090," *Archives of Materials Science and Engineering,* **99**, 1–2 (2019), 5–12.

[8] S. Kumar, D. Sethi, S. Choudhury, B. S. Roy, and S. C. Saha, "An experimental investigation to the influence of traverse speed on microstructure and mechanical properties of friction stir welded AA2050-T84 Al-Cu-Li alloy plates," *Materials Today Proceedings,* **26** (2019), 2062–2068.

[9] P. Sivaraj, D. Kanagarajan, and V. Balasubramanian, “Effect of post weld heat treatment on tensile properties and microstructure characteristics of friction stir welded armour grade AA7075-T651 aluminium alloy,” *Defence Technology*, **10** (1) (2014), 1–8.

[10] H. Sidhar and R. S. Mishra, “Aging kinetics of friction stir welded Al-Cu-Li-Mg-Ag and Al-Cu-Li-Mg alloys,” *Materials & Design*, **110** (2016), 60–71.

[11] S. Kumar, U. Acharya, D. Sethi, T. Medhi, B. S. Roy, and S. C. Saha, “Effect of traverse speed on microstructure and mechanical properties of friction-stir-welded third-generation Al–Li alloy,” *Journal of the Brazilian Society of Mechanical Sciences and Engineering*, **42** (8) (2020), 1–13.

[12] Q. Meng, Y. Liu, J. Kang, R. Dong Fu, X. Yan Guo, and Y. Jun Li, “Effect of precipitate evolution on corrosion behavior of friction stir welded joints of AA2060-T8 alloy,” *Transactions of Nonferrous Metals Society of China*, **29** (4) (2019), 701–709.

[13] J. Li, Y. Chen, X. Zhang, and Z. Zheng, “Structure and Mechanical Property of Friction-Stir Weld Joint of 2195-T8 Al-Li Alloy Plate,” *Rare Metal Materials and Engineering*, **47** (3) (2018), 780–787.

[14] J. Zhang, X. S. Feng, J. S. Gao, H. Huang, Z. Q. Ma, and L. J. Guo, “Effects of welding parameters and post-heat treatment on mechanical properties of friction stir welded AA2195-T8 Al-Li alloy,” *Journal of Materials Science & Technology*, **34** (1) (2018), 219–227.

[15] M. Mardalizadeh, M. A. Safarkhanian, and M. Khandaei, “Macro- and microstructure analysis and mechanical characteristics of thick AlMg5 alloy plates joined by floating-bobbin friction stir welding,” *Journal of Adhesion Science and Technology*, **35** (12) (2021), 1284–1304.

[16] G. Cam, S. Guczuer, A. Cakan, and H. T. Serindag, “Mechanical properties of friction stir butt-welded Al-5086 H32 plate,” *Materials Science & Engineering Technology*, **40** (8) (2009), 638–642.

[17] H. Zhang, S. B. Lin, L. Wu, J. C. Feng, and S. L. Ma, “Defects formation procedure

and mathematic model for defect free friction stir welding of magnesium alloy," *Materials & Design*, **27** (9) (2006), 805–809.

[18] P. Cavaliere, R. Nobile, F. W. Panella, and A. Squillace, "Mechanical and microstructural behaviour of 2024-7075 aluminium alloy sheets joined by friction stir welding," *International Journal of Machine Tools and Manufacture*, **46** (6) (2006), 588–594.

[19] W. F. Xu, X. K. Wu, J. Ma, H. J. Lu, and Y. X. Luo, "Abnormal fracture of 7085 high strength aluminum alloy thick plate joint via friction stir welding," *Journal of Materials Research and Technology*, **8** (6) (2019), 6029–6040.

## LIST OF PUBLICATIONS

1. **C. Shyamlal,** R. Shanmugavel, JTW Jappes, A Nair, M. Ravichandran, S. Sayath Abuthakeer, Chander Prakash, Saurav Dixit, NL Vatin, Corrosion Behavior of Friction Stir Welded AA8090-T87 Aluminum Alloy, *Materials*, 15.15 (2022): 5165.

2. **C. Shyamlal,** S. Rajesh, S. Saravana sankar, JTW Jappes, Mechanical property and microstructural evaluation of friction stir welded AA8090 T87 aluminium alloy, *Proceedings of the Institution of Mechanical Engineers, Part E: Journal of Process Mechanical Engineering* (2022): 09544089221136432..

3. **C. Shyamlal,** S. Rajesh, JTW Jappes, M. Ravichandran, S. Abuthakeer, Effects of friction stir welding process on the microstructure and mechanical properties of AA8090—T87 aluminium alloy, *Surface Topography: Metrology and Properties* 10.4 (2022): 045029.

4. **C. Shyamlal**, S. Rajesh, and S. Suresh Kumar, A comprehensive review on the effect of precipitation on mechanical properties of friction stir welded aluminium alloys, *Proceedings of the Institution of Mechanical Engineers, Part C: Journal of Mechanical Engineering Science* 235.22 (2021): 6345-6356.

**List of Conferences attended**

1. **C. Shyamlal** and S. Rajesh, “Friction stir welding: A mathematical review”, *AIP Conference Proceedings*. Vol. 2520. No. 1. AIP Publishing, 2022.